ELSEVIER

www.elsevier.nl/locate/ica

Inorganica Chimica Acta 317 (2001) 157–162

Inorganica Chimica Acta

Synthesis, crystal structure and properties of a macrocyclic dinuclear manganese(II) complex with functional *o*-methylenephenolic pendant arms

Ming Qian, Shaohua Gou *, Zhi Yu, Huangxian Ju, Yan Xu, Chunying Duan, Xiaozeng You

State Key Laboratory of Coordination Chemistry, Nanjing University, Nanjing 210093, People's Republic of China

Received 10 October 2000; received in revised form 12 January 2001

Abstract

A dinuclear manganese macrocyclic complex with functional pendant arms, $[Mn_2(II)HL^2](ClO_4)$, has been prepared by the cyclocondensation of sodium 2,6-diformyl-4-methylphenolate with *N*,*N*-bis(2-aminoethyl)-*N*-(2-hydroxybenzyl)amine and subsequent transmetallation of $Mn(II)(ClO_4)_2$. In the molecular structure of the complex, each pendant arm is bound to an adjacent manganese atom and both arms lie on the same side of the resulting tetra-imine macrocycle. Each manganese(II) ion is in a distorted octahedral configuration. The variable-temperature magnetism and the cyclic voltammogram of the complex have also been investigated. In the catalytic study, this compound exhibits a high activity for catalyzing disproportionation of H_2O_2 to O_2.

Keywords: Crystal structures; Manganese complexes; Macrocyclic complexes; Electrochemistry

1. Introduction

Manganese CAT-like activity has recently been of great interest, because manganese ions in the biosite have the ability to catalyze the disproportionation of hydrogen peroxide to dioxygen and water [1–4]. X-ray structural data of the *Thremus thermophilus* enzyme at low resolution have demonstrated that two manganese ions ligated by O and N atoms from amino acid residues are in close proximity (~ 3.6 Å) [5]. To understand further the catalytic mechanism, many functional models of manganese complexes have been made to mimic this activity [6–15]. Among them, some macrocyclic complexes with μ-phenoxo-bis[μ-carboxylate] dimanganese(II) structural species generally show a lag period in the catalytic process [16–18]. To date, however, few macrocyclic complexes with functional pendant arms have been involved in this study. Recently, we have successfully prepared a dinuclear manganese(II) complex of a pendant-arm macrocyclic ligand (H_2L^1) [19]. Experiments indicate that it can also catalyze the disproportionation of H_2O_2 to O_2, with a relatively low activity. This is presumably due to the fact that two donor atoms in each pendant arm are difficult to dissociate from the metal ion in the catalytic process. We report here on the synthesis, structure, and physico-chemical properties of a dinuclear manganese complex of a macrocyclic ligand (H_4L^2) with pendant salicyl groups, as well as on their CAT-like activities.

2. Experimental

2.1. Reagents and chemicals

The sodium salt of 2,6-diformyl-4-methylphenolate (sdmp) was prepared as reported previously [20,21]. *N*,*N* - bis(2 - Aminoethyl) - *N* - (2 - hydroxybenzyl)amine (baha) was synthesized as described previously [22]. All other solvents and chemicals were of analytical grade and used without further purification.

* Corresponding author. Tel.: +86-25-3594569; fax: +86-25-3314502.

E-mail address: sgou@nju.edu.cn (S. Gou).

0020-1693/01/$ - see front matter
PII: S0020-1693(01)00326-7

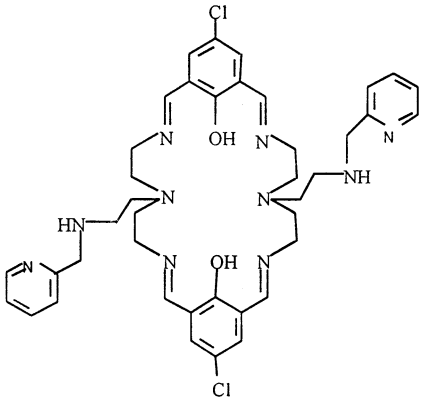

H_2L^1

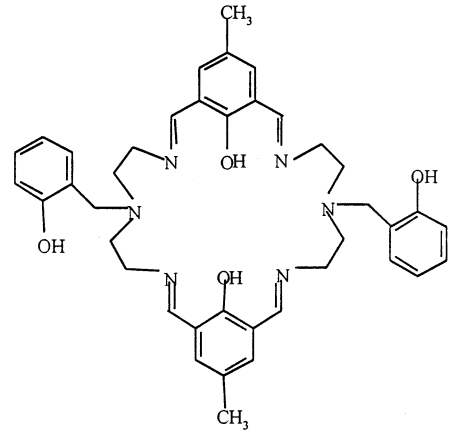

H_4L^2

Caution: although no problem was encountered in this work, transition metal perchlorates are potentially explosive and should be handled in small quantities.

2.2. Preparation of the complex

$[Mn_2(II)HL^2](ClO_4)$ was prepared by stirring an ethanol solution (50 cm^3) containing sdmp (0.19 g, 1 mmol) and baha (0.20 g, 1 mmol) at 0°C for 5 h. After removing the insoluble impurities, $Mn(ClO_4)_2 \cdot 6H_2O$ (0.36 g, 1 mmol) was added to the filtrate. The solution was refluxed for a further 2 h, then cooled to room temperature. The yellow precipitates were collected, washed with ethanol and dried over P_2O_5 in vacuo. Yield 71%. Recrystallization was undertaken in a mixed solution of CH_3CN–CH_3OH (1:1). *Anal.* Found: C, 54.39; H, 5.38; N, 9.52. Calc. for $C_{40.5}H_{45}ClMn_2N_6O_{8.5}$: C, 54.21; H, 5.02; N, 9.37%. IR (KBr, cm^{-1}): ν_{OH} 3540(s); $\nu_{C=N}$ 1648, 1632(s); $\nu_{(ClO_4)}$ 1101(vs). FAB: 675, $[H_5L^2]^+$; 781, $[Mn_2HL^2]^+$. ES–MS: 781(100%), $[Mn_2HL^2]^+$.

Table 1
Crystal and refinement data for $[Mn_2(II,II)HL^2](ClO_4) \cdot 0.5CH_3OH$

Empirical formula	$C_{40.50}H_{45}ClMn_2N_6O_{8.50}$
Formula weight	897.16
Crystal dimensions (mm^3)	$0.70 \times 0.70 \times 0.40$
Crystal system	monoclinic
Space group	$P2_1$
a (Å)	11.617(4)
b (Å)	14.005(3)
c (Å)	14.641(3)
β (°)	113.03(2)
V ($Å^3$)	2192.0(10)
Z	2
D_c ($g\,cm^{-3}$)	1.359
μ (Mo Kα) (mm^{-1})	0.694
$F(000)$	930
2θ min, max (°)	3.80, 50.00
No. of measured reflections	4242
No. of observations ($I > 2\sigma(I)$)	4034 ($R_{int} = 0.0255$)
Parameters	522
R_1, wR_2	0.0504, 0.1360
Goodness of fit	1.072
Δ (max, min) (e^- $Å^{-3}$)	0.740, −0,393

2.3. Physical measurements

Elemental analyses were performed with a Perkin–Elmer 1400C microanalyzer. IR spectra (4000–400 cm^{-1}), as KBr pellets, were recorded on a Nicolet FTIR 170X spectrophotometer. Electrospray (ES) ionization mass spectra were recorded on a Finnigan MAT SSQ 710 mass spectrometer in the scan range 300–1200 amu. Positive FAB mass spectra were measured utilizing a VG-2AB-HS mass spectrometer with NOBA as the matrix solvent. The variable-temperature (4–300 K) magnetic susceptibilities were performed in a superconducting quantum interference device (SQUID). The sample was first loaded from room temperature directly to the 6 K sample chamber in the SQUID magnetometer, and the measurement was scanned over the range 6 to 300 K by a warming mode with data corrected by the Pascal constant. A BAS-100B electrochemical analyzer (BAS Co., USA) was used for the electrochemical measurements, which were carried out under N_2 atmosphere in CH_3CN solution (approximately 1×10^{-3} mol dm^{-3}) containing tetrabutylammonium perchlorate (TBAP, 0.1 mol dm^{-3}) as the supporting electrolyte. A three-electrode system was employed with a glassy carbon working electrode, a platinum wire as auxiliary electrode and a saturated calomel electrode (SCE) as a reference electrode.

2.4. Crystal structure determination

Orange crystals of $[Mn_2(II)HL^2](ClO_4)$ suitable for

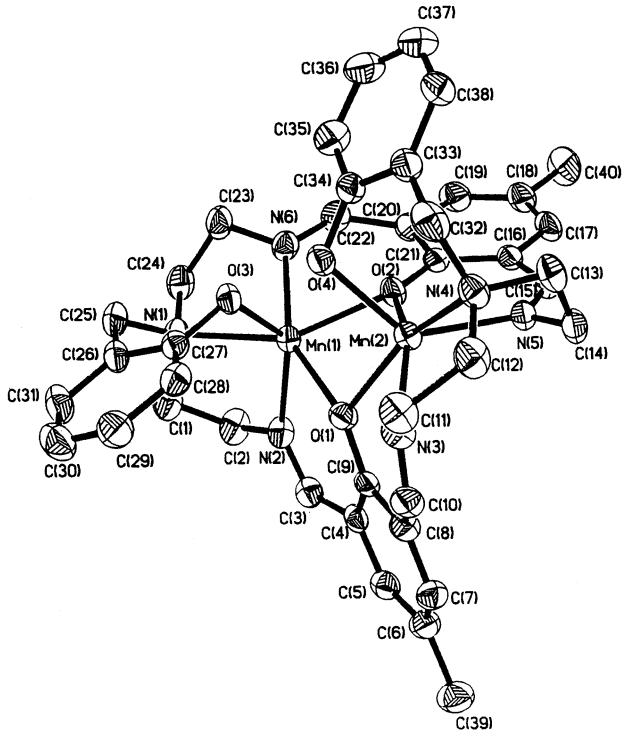

Fig. 1. An ORTEP view of the complex cation of $[Mn_2(II)HL^2](ClO_4)$.

Table 2
Selected bond lengths (Å) and angles (°) for the complex with estimated standard deviations in parentheses

Mn(1)–O(3)	2.143(3)	Mn(1)–N(2)	2.160(4)
Mn(1)–O(2)	2.195(3)	Mn(1)–O(1)	2.199(2)
Mn(1)–N(6)	2.221(3)	Mn(1)–N(1)	2.470(3)
Mn(2)–O(4)	2.133(3)	Mn(2)–N(5)	2.167(4)
Mn(2)–N(3)	2.180(3)	Mn(2)–O(1)	2.189(3)
Mn(2)–O(2)	2.213(3)	Mn(2)–N(4)	2.550(4)
O(3)–Mn(1)–N(2)	132.67(13)	O(4)–Mn(2)–N(5)	128.81(12)
O(3)–Mn(1)–O(2)	97.14(11)	O(4)–Mn(2)–N(3)	101.67(13)
N(2)–Mn(1)–O(2)	122.96(13)	N(5)–Mn(2)–N(3)	110.09(13)
O(3)–Mn(1)–O(1)	87.95(10)	O(4)–Mn(2)–O(1)	103.39(11)
N(2)–Mn(1)–O(1)	81.41(11)	N(5)–Mn(2)–O(1)	121.27(13)
O(2)–Mn(1)–O(1)	73.52(9)	N(3)–Mn(2)–O(1)	78.51(12)
O(3)–Mn(1)–N(6)	96.78(13)	O(4)–Mn(2)–O(2)	88.93(11)
N(2)–Mn(1)–N(6)	113.3(2)	N(5)–Mn(2)–O(2)	81.77(11)
O(2)–Mn(1)–N(6)	79.18(12)	N(3)–Mn(2)–O(2)	151.59(13)
O(1)–Mn(1)–N(6)	152.67(12)	O(1)–Mn(2)–O(2)	73.38(10)
O(3)–Mn(1)–N(1)	79.91(12)	O(4)–Mn(2)–N(4)	79.52(11)
N(2)–Mn(1)–N(1)	74.91(13)	N(5)–Mn(2)–N(4)	73.42(13)
O(2)–Mn(1)–N(1)	152.29(10)	N(3)–Mn(2)–N(4)	72.46(12)
O(1)–Mn(1)–N(1)	133.37(11)	O(1)–Mn(2)–N(4)	150.76(10)
N(6)–Mn(1)–N(1)	73.89(13)	O(2)–Mn(2)–N(4)	135.82(11)
Mn(2)–O(1)–Mn(1)	98.48(10)	Mn(1)–O(2)–Mn(2)	85(10)

X-ray determination were recrystallized from CH_3CN–CH_3OH (1:1) at room temperature. The crystallographic data and structural parameters are summarized in Table 1. The intensities for the complex were collected at room temperature on a Siemens P4 four-circle diffractometer with monochromated Mo Kα ($\lambda =$ 0.710 73 Å) radiation, and data reduction was carried out using XSCANS [23]. Absorption correction was applied with ψ-scan data.

The structure was solved by the direct method and refined on F^2 by full-matrix least squares. All the non-hydrogen atoms were refined anisotropically by full-matrix least squares. Hydrogen atoms were inserted in calculated positions with C–H = 0.93 Å, assigned fixed isotropic thermal parameters (1.2 times the atom to which they are attached) and allowed to ride on their respective parent atoms. All computations were carried out on a PC 586 computer using the SHELXTL-PC program package [24]. Analytical expression of neutral-atom scattering factors employed and anomalous dispersion corrections were incorporated [25].

3. Results and discussion

3.1. Synthesis and spectral characterization

The IR spectrum of the above-mentioned dry complex shows no band with the characteristic stretching frequency of the carbonyl group attributed to aldehydes and primary amine groups. However, there are strong absorption bands near 1640 cm^{-1} assigned to the imino stretching mode, proving that the cyclocondensation reaction has been completed. A strong peak in the neighborhood of 1100 cm^{-1} is ascribed to uncoordinated perchlorate groups. A band at 3540 cm^{-1} corresponding to Ar–OH has been observed, showing that at least one hydroxyl group of phenol moieties is present.

The FAB spectrum of the complex gives peaks at 675 and 781 assigned to $[H_5L^2]^+$ and $[Mn_2(II,II)HL^2]^+$, respectively, whereas the ES mass spectrum of the complex only gives a mono-charged peak at 781 attributed to $[Mn_2(II,II)HL^2]^+$. So, it is deduced from the IR spectrum, together with the elemental analysis and mass spectra data, that only one proton of phenol is present in the structure.

3.2. Crystal structure of $[Mn_2(II)HL^2](ClO_4)$

The ORTEP drawing of the molecule is shown in Fig. 1, together with the numbering scheme. Selected bond lengths and angles are listed in Table 2. The structural data reveal that this complex contains a positive and dinuclear cation, $[Mn_2HL^2]^+$, countered by a perchlorate anion with solvent molecules in disorder. In the complex cation, each metal atom is six-coordinate with an N_3O_3 unit composed of two imino nitrogen atoms, one tertiary nitrogen atom, two phenolic oxygen atoms and one oxygen atom from one of the pendant phenolic groups. It is noted that the phenolic oxygen atom of each pendant arm is bound to the adjacent manganese

atom and two pendant groups are on the same side of the macrocycle, forcing the ring to become highly twisted. Both manganese atoms have similar coordination spheres, but with a slight difference. They are bridged by two phenoxy oxygen atoms on the macrocyclic skeleton with a distance of 3.324(5) Å, which is longer than those containing bis[μ-carboxylate(halogen)] groups [16–18]. Compared with the bond length of Mn–O on the ring, the corresponding bond length on the pendant arm is a little short. The Mn–N (imino) distances, in the range 2.160 to 2.221 Å, are also shorter than those of Mn–N (tertiary) due to steric effects. The coordination geometry around each manganese atom can be described as a highly distorted octahedron. The two manganese ions are equivalent in electronic structure, which is deduced from the fact that they have similar Mn–N and Mn–O distances.

3.3. Magnetic properties

Variable-temperature magnetic susceptibility data were recorded for the complex in the temperature range 4–300 K. The $\chi_M T$ versus T plot is given in Fig. 2, and suggests an antiferromagnetic interaction between the manganese(II) ions. A model with a spin–spin interaction Hamiltonian $\boldsymbol{H} = -2J\boldsymbol{S}_1\boldsymbol{S}_2$ $(S_1 = S_2 = 5/2)$ has been used in the simulation of experimental susceptibilities using Eq. (1):

$$\chi_M = \frac{2Ng^2\beta^2}{kT} = \frac{x + 5x^6 + 14x^{12} + 30x^{20} + 55x^{30}}{1 + 3x^2 + 5x^6 + 7x^{12} + 9x^{20} + 11x^{30}} \quad (1)$$

where N is the Avogadro's number, β the Bohr moment and k the Boltzmann constant; $x = \exp(J/kT)$, where J is the exchange coupling parameter between S_1 and S_2. There was no evidence for a contribution to χ_M from a small amount of paramagnetic impurity, so a correction was not employed. As shown by the solid line in Fig. 2, the cryomagnetic behavior of the complex can be well reproduced by Eq. (1) using $J = -2.6\ \mathrm{cm}^{-1}$ and $g = 2.01$. The discrepancy factor, defined as $R = \{\Sigma|(\chi_M T)_{obsd} - (\chi_M T)_{calcd}|^2/\Sigma[(\chi_M T)_{calc}]^2\}^{1/2}$, is 2.15×10^{-2}. The exchange integral J falling in the normal range of dimeric manganese series indicates that there is a weak antiferromagnetic interaction between two manganese(II) ions.

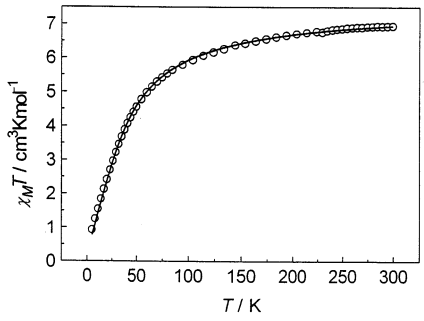

Fig. 2. $\chi_M T$ versus T plots of the complex, $[Mn_2(II)HL^2](ClO_4)$.

Table 3
Structural data for macrocyclic dinuclear $Mn_2(II,II)$ complexes

Complex	Mn–O–Mn (°)	J (cm^{-1})	Refs.
$[Mn_2(II,II)L^{3,3}(O_2CCH_3)_2]$	103.5	+0.4	[29]
$[Mn_2(II,II)HL^2(ClO_4)]$	98.4, 97.8	−2.0	this work
$[Mn_2(II,II)L^{4,4}(O_2CCH_3)_2]$	87.19	−5	[30]

It has been reported [26,27] that the bridging phenoxy Mn–O–Mn angles can be correlated with the magnitude of J. The angle at the bridging oxygen would affect the magnetic superexchange between the metal magnetic orbital and the oxygen 2p orbital. The smaller Mn–O–Mn angle would increase the ferromagnetic contribution, because it could be near orthogonal to some of the magnetic orbitals. This is contrary to the results in di-μ-phenoxo-dimanganese macrocyclic complexes listed in Table 3. The largest Mn–O–Mn angle in $[Mn_2(II)L^{3,3}(O_2CCH_3)_2]$ [28] ($L^{3,3}$ is derived from the template condensation of 2,6-diformyl-4-methylphenol with 1,3-diaminopropane) corresponds to ferromagnetic coupling between two manganese ions as they lie on opposite sides of the coplane of two basal N_2O_2 planes, leading to inefficient overlap between the manganese 3d orbitals and phenolic oxygen 2p orbitals. However, the smallest Mn–O–Mn angle in $[Mn_2(II)L^{4,4}(O_2CCH_3)_2]$ [29] ($L^{4,4}$ is derived from the condensation of 2,6-diformyl-4-methylphenol with 1,4-diaminobutane in the presence of manganese ions) results in relatively strong antiferromagnetic interaction because the two metal ions are located in the coplane of the basal N_2O_2 planes. Regarding $[Mn_2(II)HL^2](ClO_4)$, the rings are highly twisted, and each manganese ion in a distorted octahedron configuration is on the opposite side of the pendant arm, slightly deviated from the N_2O_2 plane. So the inefficient overlap between the manganese 3d orbitals and phenolic oxygen 2p orbitals produces weak antiferromagnetic coupling.

3.4. Electrochemical study

The cyclic voltammogram of the complex is shown in Fig. 3. At a scan rate of 100 mV s^{-1}, the complex shows three couples of redox peaks with peak-to-peak separation of 40 mV, 92 mV and 43 mV. The oxidation peak potentials are at 467 mV, 748 mV and 920 mV, respectively. They are consistent with a one-electron oxidation process relative to the formation of $Mn_2(II,III)$, $Mn_2(III,III)$ and $Mn_2(III,IV)$ species.

The diffusion coefficients of the complex were determined using a platinum microdisk electrode (diameter: 10 μm) based on the equation $i_d = 4nFDrc$, where i_d is

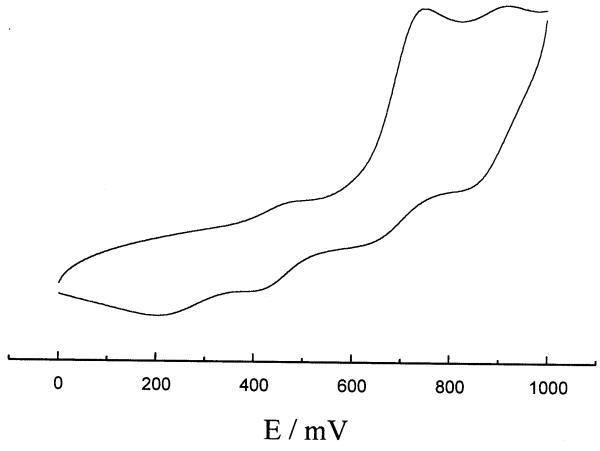

Fig. 3. Cyclic voltammogram of $[Mn_2(II)HL^2](ClO_4)$ in CH_3CN (1×10^{-3} mol dm^{-3}) containing 0.1 mol dm^{-3} NBu_4ClO_4 on a glassy carbon electrode at a scan rate of 100 mV s^{-1}.

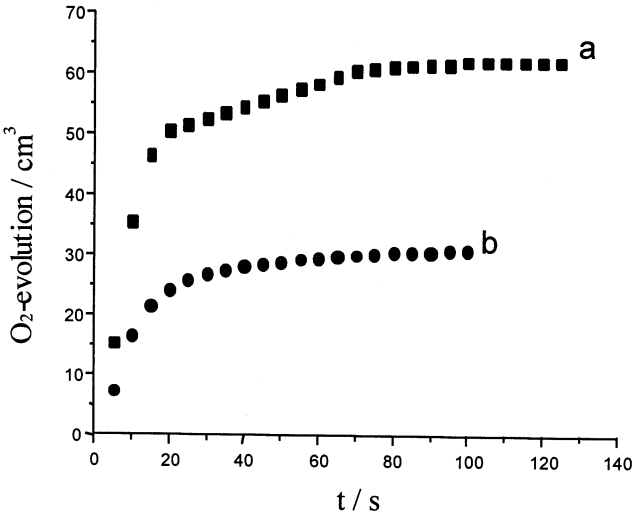

Fig. 4. Time courses of O_2 evolution in H_2O_2 decomposition by $[Mn_2(II,II)HL^2](ClO_4)$, and $[Mn_2(II,II)L^1](ClO_4)_2$: 7.8 mmol dm^{-3} of complex in 2 cm^3 CH_3CN; 8.7 mol dm^{-3} H_2O_2, in 2 cm^3 CH_3CN; (a) $[Mn_2(II,II)HL^2](ClO_4)$, (b) $[Mn_2(II,II)L^1](ClO_4)_2$.

the limiting current, r is the electrode radius, which was corrected using a CH_3CN solution containing the same concentrations of ferrocene and NBu_4ClO_4, and the other parameters have their usual meanings. The diffusion coefficient of the complex is 1.07×10^{-7} cm^2 s^{-1}, supposing the electrode reaction is a one-electron process ($n = 1$).

3.5. Catalytic activity

The course of O_2 evolution by the complex in CH_3CN at room temperature is shown in Fig. 4, together with $[Mn_2(II,II)L^1](ClO_4)_2$ under the same conditions for comparison. The H_2O_2 decomposition rate and the conversion largely depend upon the nature of the pendant arm of the macrocycles and the electronic nature of the manganese ion. 1 mol of the catalytic agent of $[Mn_2(II,II)L^1](ClO_4)_2$ could convert the 112 mol of H_2O_2 in about 2 min; meanwhile, 1 mol of $[Mn_2(II,II)HL^2](ClO_4)$ could convert 343 mol of H_2O_2 in the same time. Therefore, the catalytic activity of the title complex is comparable with that of the most efficient macrocyclic dinuclear manganese(II) complex reported [28].

The mechanism of catalyzing the disproportionation of H_2O_2 into H_2O and O_2 by dinuclear manganese complexes has been investigated by Okawa and coworkers [28,29]. It has been reported that the processes undergo an intermolecular mechanism through the interconversion of Mn(II)Mn(III)(OH) and Mn(II)Mn(IV)(=O) species, because the intermediate of Mn(II)Mn(III) and Mn(II)Mn(IV)(=O) from the reaction mixture can be detected by UV–Vis and ESR spectra [27,30]. However, the CAT-like activity of dinuclear manganese macrocyclic complexes is largely dependent upon the following factors: (i) a pair of manganese ions separated at an appropriate distance with the two vacant sites of the Mn_2 core cis to each other; (ii) labile substitution of the μ-bridging group of the complex and the nature of the macrocycle [16,18]; (iii) the equivalence in electronic nature of a pair of manganese ions [31,32].

The investigation of CAT-like activity has been made using macrocyclic dinuclear manganese(II) complexes containing bis(μ_2-carboxylate) bridging ligands [16,18]. It is proposed that dissociation of the bridging groups from the metal atom is a key step that dominates the reaction rate. Okawa and coworkers [28] have reported a macrocyclic dinuclear manganese complex, $[Mn_2L^{3,3}(OAc)_2]$, that shows high CAT-like activity. The structural study indicates that each acetate anion in the complex is bidentate to one metal atom instead of bridging two manganese ions. Its high CAT-like activity is due to the fact that the bidentate acetate group dissociates easily from the metal ion in the catalytic reaction. It is suggested that the lower activity of complexes with μ_2-bridging ligands arises from their structural inertness.

Based on the structure of $[Mn_2(II,II)HL^2](ClO_4)$, the six-coordination sphere of the metal atom is maintained by the functional pendant arm, and the bonding between the pendant arm with the manganese ion is weaker than those between the μ_2-bridging ligands and metals reported in the literature [16,18,30,33]. In addition, the pendant arm attaches to the adjacent metal ion on the same side of the ring, which has resulted in a highly twisted macrocyclic framework. The protonation of the phenoxy oxygen atom on the pendant arm has led to the rapid dissociation of the arm from the manganese ion. Thus, H_2O_2 can take advantage of the resulting empty site to carry out the CAT-like reaction at a rapid rate.

As for $[Mn_2(II,II)L^1](ClO_4)_2$, two donor atoms in one pendant arm are bonded to the adjacent metal ion, and the bond is stronger than that of the present complex. Meanwhile, the tertiary N atom in the ring is not coordinated to the manganese atom, so the ring framework is twisted less than that in the case of $[Mn_2(II,II)HL^2](ClO_4)$. As the leaving of the pendant arm from the metal ion is not easy compared with the title complex, it leads to a less efficient O_2 evolution.

4. Supplementary material

Crystallographic data have been deposited with the CCDC (12 Union Road, Cambridge, CB2 1EZ, UK) and are available on request quoting the deposition number 139141.

Acknowledgements

Thanks are due to the National Natural Science Foundation for supporting this work with grants (nos. 29871016 and 29823001) to S.G., who is also grateful for a key research grant from the State Department of Education.

References

[1] V.V. Barynin, A.I. Grebenko, Dokl. Akad. Nauk, SSSR 286 (1986) 461.
[2] (a) W. Vermaas, Annu. Rev. Plant Physiol. Plant Mol. Biol. (1990) 457. (b) R.J. Debus, Biochim. Biophys. Acta 1102 (1992) 269.
[3] O. Hausson, T. Wydrzynski, Photosynth. Res. 23 (1990) 131.
[4] K. Saner, V.K. Yachandra, R.D. Britt, M.P. Klen, in: V.L. Pecoraro (Ed.), Manganese Redox Enzymes, VCH, New York, 1992, p. 141.
[5] V.V. Barynin, A.A. Vagin, V.R. Meilk-Adamyan, A.L. Grebenk, S.V. Khangulor, A.N. Popov, M.E. Andrianova, B.K. Vainshtein, Dokl. Akad. Nauk, SSSR 288 (1986) 877.
[6] J. Pessiki, S.V. Khangulov, D.M. Ho, G.C. Dismukes, J. Am. Chem. Soc. 116 (1994) 891.
[7] P.J. Pessiki, G.C. Dismukes, J. Am. Chem. Soc. 116 (1994) 898.
[8] J. Larson, V.L. Pecoraro, J. Am. Chem. Soc. 113 (1991) 7809.
[9] Y. Naruta, K. Maruyama, J. Am. Chem. Soc. 113 (1991) 3595.
[10] Y. Naruta, M. Sasayama, T. Sasaki, Angew. Chem., Int. Ed. Engl. 33 (1994) 1839.
[11] Y. Naruta, M. Saasyama, J. Chem. Soc., Chem. Commun. (1994) 2667.
[12] U. Bossek, M. Saher, T. Weyhermueller, K. Weighardt, J. Chem. Soc., Chem. Commun. (1992) 1780.
[13] M. Watkison, A. Whiting, C.A. Mcauliffe, J. Chem. Soc., Chem. Commun. (1994) 2141.
[14] C. Higuchi, H. Sakiyama, H. Okawa, R. Isobe, D.E. Fenton, J. Chem. Soc., Dalton Trans. (1994) 1097.
[15] H. Sakiyama, H. Okawa, R. Isobe, J. Chem. Soc., Chem. Commun. (1993) 882.
[16] T. Nagata, Y. Ikawa, K. Maruyama, J. Chem. Soc., Chem. Commun. (1994) 471.
[17] T. Aono, H. Wada, M. Yonemura, M. Ohba, H. Okawa, D.E. Fenton, J. Chem. Soc., Dalton Trans. (1997) 1527.
[18] T. Nagata, J. Mizukami, J. Chem. Soc., Dalton Trans. (1995) 2825.
[19] M. Qian, S. Gou, S. Chantrapromma, S.S.S. Raj, H.-K. Fun, Q. Zeng, Z. Yu, X. You, Inorg. Chim. Acta 305 (2000) 83.
[20] S. Gou, D.E. Fenton, Inorg. Chim. Acta 223 (1994) 169.
[21] Z. Zeng, J. Sun, S. Gou, K. Zhou, J. Fang, H. Chen, Transition Met. Chem. 23 (1998) 371.
[22] Q. Zeng, M. Qian, S. Gou, H.-K. Fun, X. You, Inorg. Chim. Acta 294 (1999) 1.
[23] Siemens, XSCANS (Version 2.1), Siemens Analytical X-Ray Instruments Inc., Madison, USA, 1994.
[24] Siemens, SHELXTL (Version 5.0), Siemens Industrial Automation Inc., Analytical Instrumentation, USA, 1995.
[25] A.J.C. Wilson (Ed.), International Tables for X-Ray Crystallography, vol. C, Kluwer, Dordrecht, 1992, pp. 500–502 (Table 6.1.1.4), pp. 219–222 (Table 4.2.6.8) and pp. 193–199(Table 4.2.4.2).
[26] P.A. Vigato, S. Tamburini, D.E. Fenton, Coord. Chem. Rev. 106 (1990) 25.
[27] A.R. Schake, E.A. Schmitt, A.J. Conti, W.E. Streib, J.C. Huffman, D.N. Hendrickson, G. Christoll, Inorg. Chem. 30 (1991) 3192.
[28] H. Wada, K. Motoda, M. Ohba, H. Sakiuama, N. Matsumoto, H. Okawa, Bull. Chem. Soc., Jpn. 68 (1995) 1105.
[29] T. Aono, H. Wada, M. Yonemura, M. Ohba, H. Okawa, D.E. Fenton, J. Chem. Soc., Dalton Trans. (1997) 1527.
[30] H. Sakiyama, H. Okawa, M. Suzuki, J. Chem. Soc., Dalton Trans. (1994) 1097.
[31] H. -R. Chang, S.K. Larsen, P.D.W. Boyd, C.G. Pierpont, D.N. Hendrickson, J. Am. Chem. Soc. 110 (1988) 4565.
[32] H. Okawa, H. Sakiyama, Pure Appl. Chem. 67 (1995) 273.
[33] H. Sakigama, H. Okawa, R. Isobe, J. Chem. Soc., Chem. Commun. (1993) 882.